ChemPubSoc Europe

DOI: 10.1002/chem.201600984

CHEMISTRY A European Journal Full Paper

Host–Guest Systems |*Hot Paper*|

# Star-Shaped Conjugated Molecules with Oxa- or Thiadiazole Bithiophene Side Arms

Kamil Kotwica,[a] Anastasia S. Kostyuchenko,[b, c] Przemyslaw Data,[d] Tomasz Marszalek,[e] Lukasz Skorka,[a] Tomasz Jaroch,[f] Sylwia Kacka,[a] Malgorzata Zagorska,[a] Robert Nowakowski,[f] Andrew P. Monkman,[d] Alexander S. Fisyuk,*[b, c] Wojciech Pisula,*[e, g] and Adam Pron*[a]

**Abstract:** Star-shaped conjugated molecules, consisting of a benzene central unit symmetrically trisubstituted with either oxa- or thiadiazole bithiophene groups, were synthesized as promising molecules and building blocks for application in (opto)electronics and electrochromic devices. Their optical ($E_g$(opt)) as well as electrochemical ($E_g$(electro)) band gaps depended on the type of the side arm and the number of solubilizing alkyl substituents. Oxadiazole derivatives showed $E_g$(opt) slightly below 3 eV and by 0.2 eV larger than those determined for thiadiazole-based compounds. The presence of alkyl substituents in the arms additionally lowered the band gap. The obtained compounds were efficient electroluminophores in guest/host-type light-emitting diodes. They also showed a strong tendency to self-organize in monolayers deposited on graphite, as evidenced by scanning tunneling microscopy. The structural studies by X-ray scattering revealed the formation of supramolecular columnar stacks in which the molecules were organized. Differences in macroscopic alignment in the specimen indicated variations in the self-assembly mechanism between the molecules. The compounds as trifunctional monomers were electrochemically polymerized to yield the corresponding polymer network. As shown by UV/Vis-NIR spectroelectrochemical studies, these networks exhibited reversible electrochromic behavior both in the oxidation and in the reduction modes.

## Introduction

Star-shaped conjugated molecules containing oligothiophenes in their side arms began to draw interest of chemists and physicists nearly 20 years ago[1] due to distinctly different properties as compared to their linear analogues (see, for example, ref. [2]). This involved, among others, improved solution processability, interesting electrochemistry, and promising electrical transport properties. These molecules usually consist of an aromatic, heteroaromatic or triphenylamine core to which oligothiophene or donor/acceptor-type groups with thiophene rings are radially attached. Benzene is probably the most popular aromatic core,[1,3–7] however, more extended cores should also be mentioned such as truxene.[8,9] Star-shaped molecules with heterocyclic cores such as triazine are also reported.[1,11,12] Larger cores containing heterocycles are frequently built from fused aromatic and heterocyclic rings such as benzodithiophene,[13] benzotrithiophene,[14–16] or phenylquinoxaline.[17] Star-shaped compounds with triphenylamine-type cores, inducing non- planarity of the molecule, were also synthesized.[18–25] It should be mentioned that the triazine core can play the role of an electron accepting unit to which arms with electro-donating groups are attached, whereas, inversely, arms containing electro-accepting units can be attached to an electro-donating core.[20,22]

Star-shaped molecules with thienylene (or thienyl) groups frequently show interesting optical properties including photoluminescence of high quantum yield,[19] solvatochromism,[12] and electrochromism.[26] They are electrochemically active[1,7,11] and can form a 3D network through electrochemical polymerization.[9,15,26] Due to good electrical transport properties they

[a] K. Kotwica, L. Skorka, S. Kacka, Prof. M. Zagorska, Prof. A. Pron
Faculty of Chemistry, Warsaw University of Technology
Noakowskiego 3, 00664, Warsaw (Poland)
E-mail: apron@ch.pw.edu.pl

[b] A. S. Kostyuchenko, Prof. A. S. Fisyuk
Department of Organic Chemistry, Omsk F. M. Dostoevsky State University
Mira av. 55A, Omsk (Russian Federation)
E-mail: fisyuk@chemomsu.ru

[c] A. S. Kostyuchenko, Prof. A. S. Fisyuk
Laboratory of New Organic Materials, Omsk State Technical University
Mira av. 11, Omsk , 644050 (Russian Federation)

[d] Dr. P. Data, Prof. A. P. Monkman
Physics Department, University of Durham
South Road, Durham , DH1 3LE (United Kingdom)

[e] Dr. T. Marszalek, Prof. W. Pisula
Max Planck Institute for Polymer Research
Ackermannweg 10, 55128 Mainz (Germany)
E-mail: pisula@mpip-mainz.mpg.de

[f] Dr. T. Jaroch, Prof. R. Nowakowski
Institute of Physical Chemistry, Polish Academy of Sciences
Kasprzaka 44/52, 01224 Warsaw (Poland)

[g] Prof. W. Pisula
Department of Molecular Physics, Faculty of Chemistry
Lodz University of Technology, Zeromskiego 116, 90-924 Lodz (Poland)

Supporting information for this article can be found under http://dx.doi.org/10.1002/chem.201600984.

can also serve as components of active layers in organic field-effect transistors.[3,4,8,23] However, the largest effort was directed towards the application of these semiconductors (especially those of donor/acceptor character) in bulk heterojunction-type organic photovoltaic cells.[5,16,17,22,25,27]

In this paper we report on new, solution-processable star-shaped molecules with benzene central core to which donor/acceptor-type side arms are attached consisting of either oxa- or thiadiazole bithiophene groups. We demonstrate that the redox properties of these molecules can be tuned not only by the chemical nature of the acceptor unit but also by the number and the position of the solubilizing alkyl substituents. Capability of self-assembling into highly ordered 2D monolayers is another interesting feature of these new compounds as well as their molecular topology-dependent 3D supramolecular organization in extruded fibers. We also show that they can be applied as electroluminophores in guest/host-type light-emitting diodes (LEDs). The use of star-shaped donor/acceptor molecules as emitters in LEDs is rare, although it was reported for star molecules containing oxadiazole and carbazole units in their arms[28] and in carbazole dendrimers with a fluorinated phenylene oxadiazole core.[29] Finally, we prove that the new

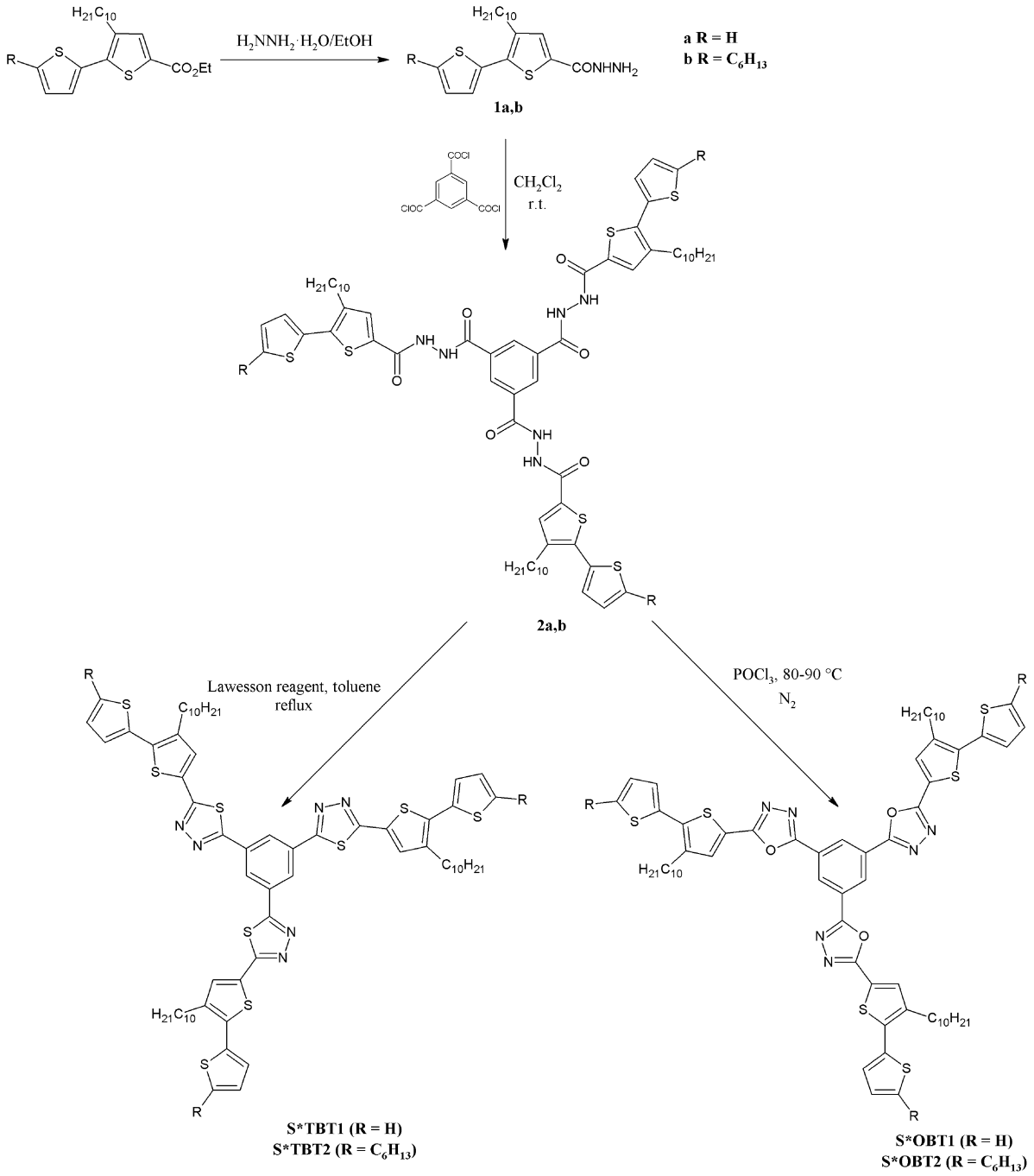


**Scheme 1.** Synthetic route to star-shaped molecules containing either thiadiazole- or oxadiazolebithiophene side arms.

molecules can serve as trifunctional monomers yielding polymer networks upon their electrochemical polymerization. These networks show reversible electrochromism both in the oxidation and in the reduction modes.

## Results and Discussion

### Synthesis

The star-shaped molecules were prepared from ethyl ester of alkyl-substituted 2,2′-bithiophene-5-carboxylic acid in three steps (Scheme 1). In the preparation of the compounds the procedure described by Kostyuchenko et al.[30] (based on a modification of the Fiesselmann reaction) was followed. The ester was converted into the corresponding hydrazide derivative (**1 a,b**) by heating hydrazine monohydrate at reflux in alcohol. Treatment of **1 a,b** with benzene-1,3,5-tricarboxylic (trimesic) acid chloride yielded alkyl-substituted $N'^1$,$N'^3$,$N'^5$-tris[(3-decyl-2,2′-bithien-5-yl)carbonyl]benzene-1,3,5-tricarbohydrazides (**2 a,b**). These compounds **2 a,b** were converted into the final products of the oxadiazole bithiophene series, that is, 2,2′,2′′-benzene-1,3,5-triyltris[5-(2,2′-bithien-5-yl)-1,3,4-oxadiazoles], termed in the subsequent text as **S*OBT1** and **S*OBT2**, in the reaction with phosphorus oxychloride.[31] Treatment of **2 a,b** with Lawesson's reagent resulted in their conversion into 2,2′,2′′-benzene-1,3,5-triyltris[5-(2,2′-bithien-5-yl)-1,3,4-thiadiazoles], that is, compounds of the thiadiazole bithiophene series (**S*TBT1** and **S*TBT2**) in good yields. The detailed description of the synthesis of all compounds described in this paper, together with their spectroscopic characterization (NMR, IR) and elemental analysis can be found in the Supporting Information.

### Absorption and emission spectroscopy

Absorption spectra of all four compounds are presented in Figure 1 a whereas their principal optical parameters are collected in Table 1. All spectra are characterized by a dominant, unresolved band ascribed to the π–π* transition in the conjugated system. Note that the π–π* bands of the thiadiazole derivatives (**S*TBT1** and **S*TBT2**) are bathochromically shifted by 27 nm as compared to the same bands in the corresponding oxadiazole compounds, that is, **S*OBT1** and **S*OBT2**. This is associated with stronger aromaticity of thiadiazole as compared to oxadiazole and improved conjugation in the compounds of the **S*TBT** series. Aromatic stabilization energy of thiadiazole is nearly twice higher than that of oxadiazole.[32,33] Its stronger aromaticity is also manifested in higher values of the harmonic oscillator measure of aromaticity (HOMA) indices[34] calculated for the thiadiazole derivatives as compared to the corresponding oxadiazole ones.[33,35] One should additionally note that the position of the π–π* band is also dependent on the number of alkyl solubilizing groups, being bathochromically shifted by 12 nm for the derivatives with two alkyl substituents in each arm. The same effect of alkyl substituents on molecular planarization (as evidenced from B3LYP/6-31G* calculations) and on their increase in aromaticity (determined by the bond length alternation (BLA) parameter) was reported for penta-ring linear compounds constituted of a central tetrazine,[36] thiadiazole[37] or oxadiazole[38,39] electron accepting group symmetrically disubstituted with alkyl- or dialkylbithiophenes. As a result, weak positive inductive effect of alkyl substituents leads to lowering of the optical gap.

Although trisubstituted benzene as the central unit of the studied star-shaped molecules should assure their good planarity and conjugation, the planarity-sensitive π–π* band in the spectra of these molecules is hypsochromically shifted by 13 to 16 nm, as compared to the case of the corresponding linear oxa- or thiadiazoles disubstituted with either alkylbithiophene or dialkylbithiophene.[37,39,40]

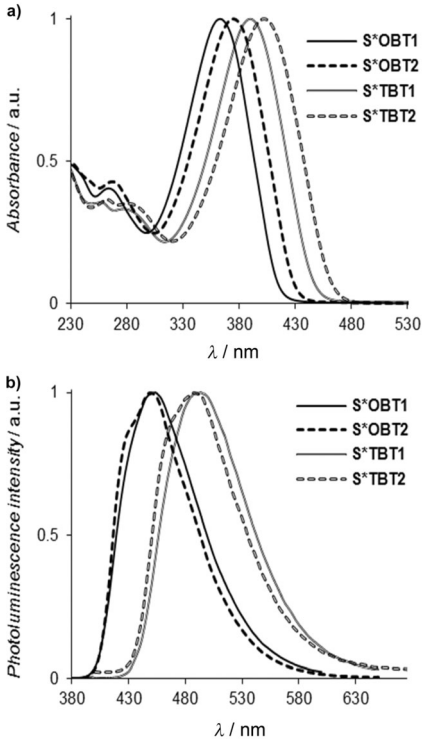


**Figure 1.** a) Solution ($CH_2Cl_2$ solvent) absorption spectra of **S*TBT1**, **S*TBT2**, **S*OBT1** and **S*OBT2**; b) solution ($CH_2Cl_2$ solvent) emission spectra of **S*TBT1**, **S*TBT2**, **S*OBT1** and **S*OBT2** ($\lambda_{exc}=\lambda_{max}$ abs).

**Table 1.** UV/Vis and photoluminescence spectroscopic parameters of the studied star-shaped molecules.

| | $\lambda_{max}$ (absorption, $CH_2Cl_2$ solution) [nm] | $\lambda_{max}$ (absorption, thin film) [nm] | $\lambda_{max}$ (emission, $CH_2Cl_2$ solution)[a] [nm] | Stokes shift [nm] | Quantum yield [%] | $E_g$(opt) [eV] |
|---|---|---|---|---|---|---|
| **S*OBT1** | 363 | 381 | 453 | 90 | 33 | 2.98 |
| **S*OBT2** | 375 | 376 | $434_{(shoulder)}$,449 | 59 | 23 | 2.88 |
| **S*TBT1** | 390 | 398 | 494 | 104 | 15 | 2.77 |
| **S*TBT2** | 402 | 404 | $473_{(shoulder)}$, 488 | 71 | 14 | 2.68 |

[a] $\lambda_{exc}=\lambda_{max}$ abs.

The π–π* band in the thin film spectra of molecules containing one alkyl solubilizing group in each arm (**S*TBT1** and **S*OBT1)** is bathochromically shifted with respect to the position of this band in the solution spectra (see Table 1). This means that lower planarity of these molecules in solution has its origin in the interaction with the solvent molecules and in the solid state this planarity is improved. This effect is not observed in the case of molecules containing two alkyl groups per arm (**S*TBT2** and **S*OBT2)** whose solution and solid state spectra are very similar. Evidently, their better planarity in the solution is not being further improved in the solid state. Solid state spectra of all four molecules studied are presented in the Figure S1 of the Supporting Information.

Photoluminescence spectra of **S*TBT1** and **S*OBT1**, that is, molecules with one solubilizing alkyl substituent in each arm are featureless similarly as their absorption spectra (see Figure 1 b). Vibrational structure, although not very highly pronounced, is observed in the emission spectra of molecules with two alkyl substituents (**S*TBT2** and **S*OBT2)**, which may be interpreted in terms of some rigidification of the molecular structure in the excited state, possibly through benzoid-quinoid type of transformation occurring upon excitation.[41] Relatively large Stokes shifts are measured for **S*TBT1** and **S*OBT1**, 90 and 104 nm, respectively. They are larger than the shifts reported for the corresponding linear compounds containing oxadiazole or thiadiazole units[37–40] and additionally corroborate significant, excitation-induced changes in their molecular structure. Smaller Stokes shifts are found for **S*TBT2** and **S*OBT2** (59 and 71 nm) comparable to those noted for the linear compounds.

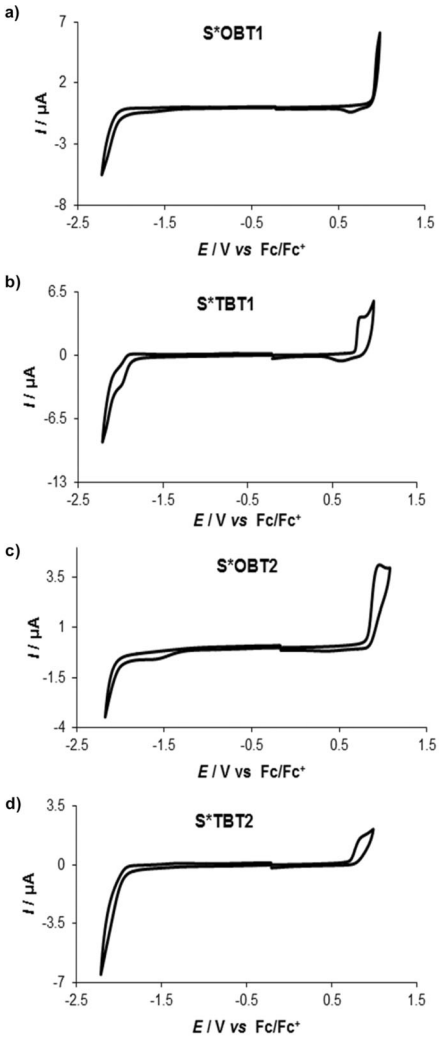


**Figure 2.** Cyclic voltammograms of the studied star-shaped molecules (concentration $5\times10^{-4}$ M in 0.1 M $Bu_4NPF_6/CH_2Cl_2$; scan rate: 50 mV $s^{-1}$).

## Electrochemistry

Figure 2 shows cyclic voltammograms of all four molecules. It is known that thiophene-capped conjugated molecules are capable of electropolymerizing by $C_\alpha$–$C_\alpha$ oxidative coupling. Although the presence of an electro-accepting group such as oxadiazole or thiadiazole in the monomer shifts the oxidative polymerization potential to higher values, the electropolymerization is still possible, provided that the terminal thiophene ring is separated from the acceptor unit by an additional thienylene spacer.[43,44] **S*OBT1** and **S*TBT1** whose $C_\alpha$ position in the terminal thienyl ring is not blocked by an alkyl substituent, also electropolymerize. However, since both compounds are trifunctional monomers a polymer network is formed rather than a linear chain. At the vertex potential the formed polymer is in its oxidized (polycationic) state and its reduction to the neutral state is manifested by a cathodic peak appearing in the cyclic voltammogram upon the reverse scan (Figure 2 a, b). Note that no cathodic peaks are present in the voltammograms of **S*OBT2** and **S*TBT2** (Figure 2 c, d) whose polymerization is impeded by blocking the $C_\alpha$ positions, with alkyl groups. Thus, in these cases the polymerization through $C_\alpha$–$C_\alpha$ coupling is impossible and other types of couplings are highly improbable, due to the steric reasons. For both compounds the radical cations formed at relatively high potentials are very reactive and undergo consecutive reactions of chemical nature, leading to oxidative degradation of the molecules, which is manifested in a partial or total loss of their electrochemical activity. The same behavior was previously observed in the case of linear monomers consisting of oxiadiazole or thiadiazole disubstituted with alkylbithiophene groups.[38,43] The reduction process of all four molecules is irreversible, similarly as linear oxa- and thiadiazoles disubstituted with alkyl- or dialkylbithiophenes (Figure 2).[37,39,40] Molecules containing thiadiazole electron withdrawing units are easier to reduce and easier to oxidize as compared to their oxadiazole analogues (see Figure 2 and data presented in Table 2) yielding lower ionization potential (IP) and higher electron affinity (EA) values. As a result, the electrochemical gaps ($E_g$(electro)) of **S*TBT1** and **S*TBT2** are smaller than those of **S*OBT1** and **S*OBT2**. The trend is similar as in the case of linear donor–acceptor compounds consisting of the same electron-withdrawing and -donating groups, however, in the star-shaped molecules the electrochemical band gaps are smaller by 120 to 170 meV.[39,40]

**Table 2.** Electrochemical parameters of the studied star-shaped molecules derived from cyclic voltammograms.

| Compound | $E_{ox,onset}$ [V] | $E_{red,onset}$ [V] | IP[a] [eV] | EA[b] [eV] | $E_g$ (electro) [eV] |
|---|---|---|---|---|---|
| **S*OBT1** | 0.900 | −2.010 | 5.700 | −2.790 | 2.91 |
| **S*OBT2** | 0.820 | −1.990 | 5.620 | −2.810 | 2.81 |
| **S*TBT1** | 0.770 | −1.875 | 5.570 | −2.925 | 2.65 |
| **S*TBT2** | 0.715 | −1.960 | 5.515 | −2.840 | 2.68 |

[a] Calculated according to equation: IP (eV) = |e|($E_{ox,\ onset}$ + 4.8), [b] Calculated according to equation EA (eV) = −|e|($E_{red,\ onset}$ + 4.8)

**Table 3.** Molecular orbital energies along with ionization potential (IP) and electron affinity (EA) calculated in solution at B3LYP/6-31G(d,p) level of theory.

| Compound | HOMO [eV] | LUMO [eV] | IP [eV] | EA [eV] |
|---|---|---|---|---|
| **S*OBT1** | −5.65 | −2.14 | 5.56 | −2.41 |
| **S*OBT2** | −5.47 | −2.05 | 5.42 | −2.38 |
| **S*TBT1** | −5.57 | −2.30 | 5.76 | −2.60 |
| **S*TBT2** | −5.40 | −2.21 | 5.36 | −2.52 |

### DFT calculations

DFT calculations were carried out with the goal to confront theoretical predictions with the experimental findings. In particular, they covered molecular orbital localization versus spin density distribution, ionization potential (IP) and electron affinity (EA) values as well as vertical excitations. This is illustrated in Figure 3a,b where the frontier orbitals of **S*OBT1** and **S*TBT1** are presented. The frontier orbitals of **S*OBT2** and **S*TBT2** are depicted in Figure S2 of the Supporting Information. In both cases the HOMO orbitals are localized on the bithiophene moieties, pushed towards the edges of the molecule, whereas the LUMO ones are mainly spread over the central benzene ring and the adjacent oxadiazole or thiadiazole units. The calculated HOMO and LUMO energies are listed in Table 3.

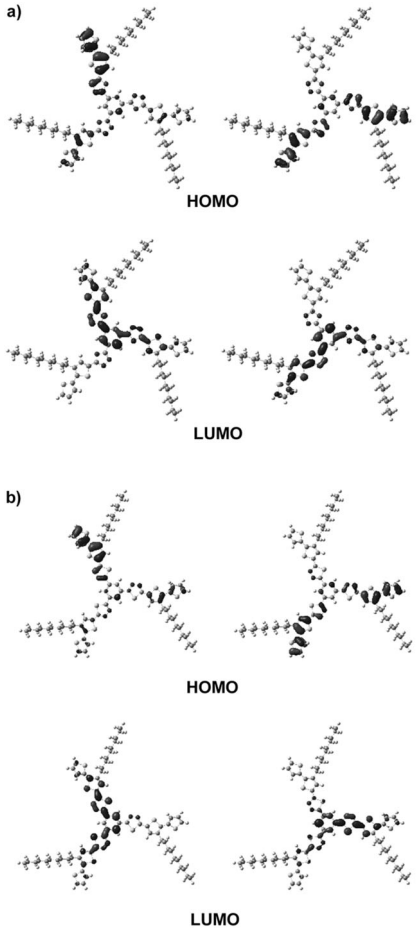


**Figure 3.** Molecular orbital contours obtained at B3LYP/6-31G(d,p) level of theory (isosurface value = 0.03); a) **S*OBT1**; b) **S*TBT1**.

Figure 4a,b show the unpaired spin density distribution in the radical anion and radical cation forms of **S*OBT1** and **S*TBT1**. The obtained spin density contours can be considered as a superposition of the corresponding HOMO or LUMO contours and prove that the unpaired electron is evenly delocalized over the molecular backbone. For **S*OBT2** and **S*TBT2** very similar data are obtained (see Figure S3 in the Supporting Information).

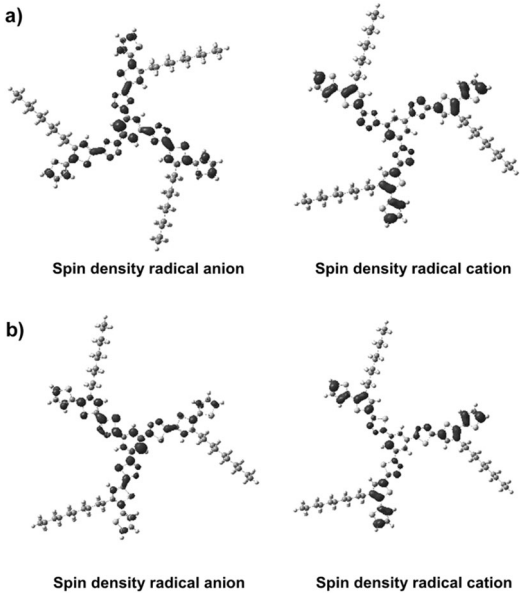


**Figure 4.** Spin density contours of radical cation and radical anion at B3LYP/6-31G(d,p) level of theory (isosurface value = 0.0004); a) **S*OBT1**; b) **S*TBT1**

Vertical excitations contributing to the electronic transitions were analyzed using the TD-DFT approach. For the most significant transitions (osc. strength > 0.1) Natural Transition Orbital (NTO) analysis was performed to better understand their origin. In all cases, due to symmetry constrains, the ground-to-first-excited-state transition was highly privileged (respective NTOs are presented in Tables S2 to S5 in the Supporting Information). For the oxadiazole derivatives (**S*OBT1** and **S*OBT2**) this transition was a mixture of charge transfer from end-capped bithiophenes to the central benzene ring with some small contribution of oxadiazole. In the case of thiadiazole-sub-

stituted derivatives the first transition was mainly a charge transfer from the bithiophene moiety to the thiadiazole one as revealed by NTO eigenvalues. The same trend was observed in the experimentally measured and theoretically calculated electronic transitions, the latter were consistently less energetic by 0.27 eV. IP values determined experimentally from the cyclic voltammetry measurements are close to those calculated using DFT at B3LYP/6-31G(d,p) level of theory. Higher differences between the measured and calculated values are found for EA. However, both trends are very similar (compare data collected in Tables 2 and 3).

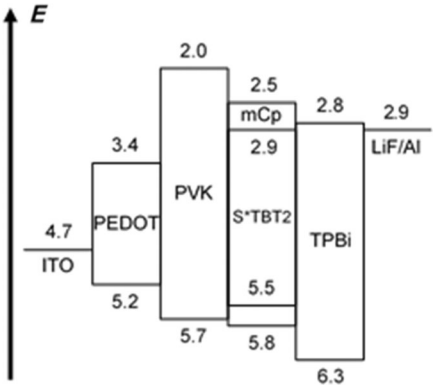


**Figure 5.** Device structure and energy diagram of the studied guest/host light-emitting diodes. PEDOT = poly(3,4-ethylenedioxythiophene); PVK = poly(9-vinylcarbazole); mCP = 1,3-bis(N-carbazolyl)benzene; TPBi = 2,2′,2′′-(1,3,5-benzinetriyl)-tris(1-phenyl-1-H-benzimidazole).

### Electroluminescence and light-emitting diodes

The investigated derivatives combine solution processability with luminescent properties. We were therefore tempted to verify whether it is possible to fabricate light-emitting diodes (LEDs) through solution processing. We chose the guest–host configuration for the emissive layer.[45] In this type of diode, "guest" luminescent molecules (usually few percent) are dispersed in a host matrix, which consists of one or two organic semiconductors of a relatively wide energy gap. Singlet excitons formed in the host matrix as a result of electron and hole injection from the electrodes are then transferred to the guest molecule through the Förster energy transfer. Then they recombine emitting a photon. Förster energy transfer requires partial overlap of the host emission spectrum and the guest absorption spectrum.

An alternative mechanism of the electroluminescence, involving charge carrier trapping can also be envisioned in this type of emissive layers. If the LUMO level of the guest molecule is lower than that of the host and, in addition, the HOMO level of the guest is higher than that of the host, the guest molecules constitute traps for both types of charge carriers injected to the matrix from the electrodes and the excitons can be formed directly on the guest molecule without the necessity of the charge transfer from the host matrix to the guest luminophore.[46]

Devices of the following structure were fabricated: ITO/PEDOT:PSS/PVK/S*TBT2 (or S*OBT2)-mCP/TPBi/LiF/Al. The energy levels alignment of all diode components is schematically presented in Figure 5. The electroluminescence bands registered for emissive layers containing 1 wt% of **S*TBT2** or **S*OBT2** are featureless and show clear maxima at 475 nm and 520 nm, respectively. Note that the electroluminescence bands are bathochromically shifted by about 30 nm with respect to the corresponding bands in the solution photoluminescence spectra (see Table 1). Both compounds exhibit diode-like behavior with the turn on voltage of ≈7 V as evidenced by their current and luminance versus voltage characteristics shown in Figure 6a,b. The luminance values exceeding 1800 cd m$^{-2}$ and luminous efficiencies approaching 3.5 cd A$^{-1}$ were measured for diodes with 1 wt% **S*TBT2** emitter. The highest external quantum efficiency (EQE) of 1.35% was measured for the luminance of about 500 cd m$^{-2}$ but it never dropped below 0.8% for the whole range of higher luminances (see Figure 6c). The external

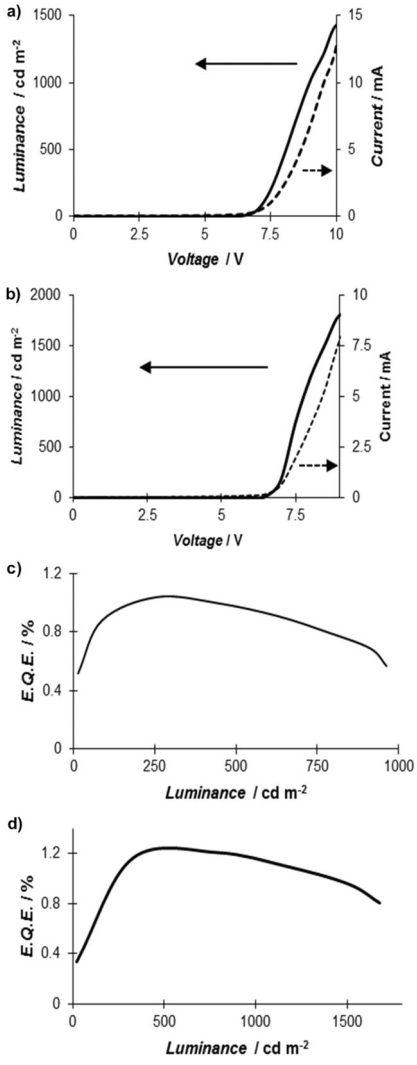


**Figure 6.** a) Current versus voltage and luminance versus voltage characteristics for diode with active layers containing with 1 wt% of **S*OBT2**; b) current versus voltage and luminance versus voltage characteristics for diode with active layers containing with 1 wt% of **S*TBT2**; c) external quantum efficiency versus luminance for diode with active layers containing with 1 wt% of **S*OBT2**; d) external quantum efficiency versus luminance for diode with active layers containing with 1 wt% of **S*TBT2**.

**Table 4.** Electroluminescence data for diodes containing **S*TBT2** and **S*OBT2** dispersed in 1,3-bis(N-carbazolyl)benzene (mCP) matrix (1–15 wt%).

| | S*TBT2 | | S*OBT2 | |
|---|---|---|---|---|
| | [cd m$^{-2}$][a] | [cd A$^{-1}$][b] | [cd m$^{-2}$] | [cd A$^{-1}$] |
| **1 wt%** | 1803 | 3.43 | 1428 | 1.67 |
| **3 wt%** | 1847 | 2.85 | 1438 | 1.74 |
| **5 wt%** | – | – | 1229 | 1.76 |
| **10 wt%** | 1028 | 2.14 | 434 | 0.94 |
| **15 wt%** | 508 | 2.02 | 531 | 1.01 |

[a] Luminance; [b] Luminous efficiency.

quantum and luminous efficiencies of diodes containing 1 wt% of **S*OBT2** were 30% lower (see Figure 6d and Table 4).

We have tested the effect of the electroluminophore content in the mCP matrix on the electroluminescence parameters of the fabricated diodes. The results are collected in Table 4. For the emitter contents of 1% and 3% the diode parameters are comparable, whereas for its higher contents they worsen. This effect can be considered as a manifestation of nanoaggregation of the electroluminophore at its higher contents that favors the non-radiative quenching.

### Self-assembly and supramolecular organization in monolayers and in bulk

Low molecular mass organic semiconductors containing alkyl substituents can exhibit a strong tendency to self-organize in monolayers deposited on appropriate substrates. This is also the case of linear compounds of thiadiazole or tetrazine disubstituted with alkyl- or dialkylbithiophenes.[37,47] Intrinsic threefold symmetry of star-shaped thia- or oxadiazole bithiophene molecules described here, together with the same type of symmetry of the graphene layer, should facilitate the formation of ordered 2D supramolecular structures on highly oriented pyrolytic graphite (HOPG) substrates. Our attempts to obtain ordered monomolecular layers showed that star-shaped molecules containing thiadiazole units have a stronger tendency to self-organize on HOPG than their oxadiazole analogues. Monolayers of **S*TBT1** and **S*TBT2** form 2D polycrystals in which large, ordered domains of the size of few hundreds nanometers, differing in their orientation, can be distinguished. STM images of **S*OBT1** and **S*OBT2** reveal smaller isolated ordered domains embedded in an amorphous matrix. Figure 7a shows a representative STM image of a particular 2D domain of self-assembled **S*TBT1** molecules.

The image of one domain is characterized by a hexagonal network of black spots, attributable to regularly spaced molecular cavities. The cavities are separated from each other in three directions by the same distance of (2.8 ± 0.2) nm. Based on the geometrical features of the observed STM image, a plausible model of the molecules adsorption geometry can be obtained using the HyperChem software package (see Figure 7b). According to this model, hexagonally packed **S*TBT1** molecules constitute a molecular network of triangles in which every second triangle is empty forming a molecular cavity

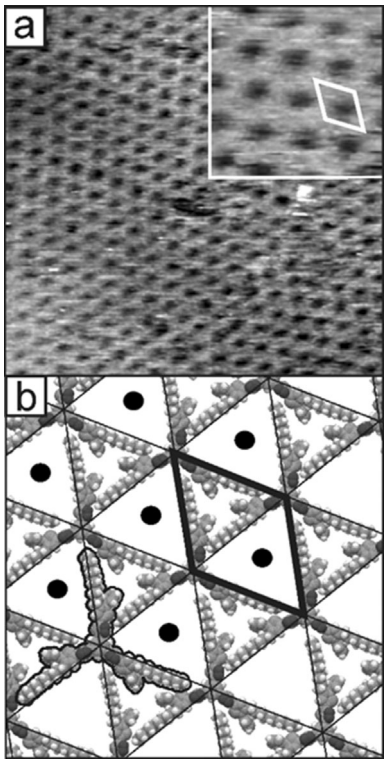


**Figure 7.** a) STM image and b) the proposed adsorption geometry of a monolayer of **S*TBT1** on HOPG. Scanning area and the measurement parameters: a) 46×46 nm$^2$ (zoom image 11×11 nm$^2$); $V_{bias}$ (tip) = 1.1 V, $I_t$ = 0.3 nA.

(marked in Figure 7b by black dots). The remaining triangles are "filled" with three arms of three neighboring molecules. The empty cavities are visible in the STM image as regularly spaced black spots distant by 2.8 nm, that is, by the distance corresponding to the intermolecular separation.

Besides the monolayer assembly, the bulk organization of the compounds was also studied. All four compounds are crystalline at ambient temperatures exhibiting one phase transition in the differential scanning calorimetry (DSC) scans attributed to the melting point. The melting temperature varies with the number of alkyl side chains from 147.6 °C and 132.6 °C for **S*OBT1** and **S*TBT1**, respectively, to 99.9 °C and 110.2 °C for **S*OBT2** and **S*TBT2**. As expected, the higher the number of substituents is attached, the lower the phase transition temperature is found. The supramolecular organization in bulk was investigated by two-dimensional wide-angle X-ray scattering (2D-WAXS) on macroscopically aligned fiber samples. These samples were prepared by mechanical extrusion, which induced macroscopic orientation of the molecules. For the measurements, which were performed at 30 °C, the samples were mounted vertically in front of the 2D detector.

Figure 8 shows the 2D patterns of the four compounds confirming by the high number of distinct reflections their crystalline nature. Although the unit cells could not be clearly identified due to this large number of scattering intensities, distinct differences in the supramolecular organization between the compounds is evident from the patterns. For this reason, the analysis was focused on the influence of the molecular design

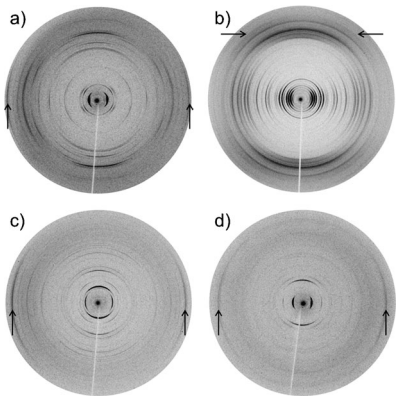


**Figure 8.** 2DWAXS patterns of a) **S*OBT1**, b) **S*OBT2**, c) **S*TBT1** and d) **S*TBT2** recorded at 30 °C. The fibers were placed vertically in front of the detector. Arrows indicated the π-stacking reflections.

on the organization in the fiber samples rather than on the crystallographic parameters. All four compounds self-assemble in one-dimensional columnar stacks similar to other star-shaped molecules.[48–54] The pattern of **S*OBT2** displays a typical distribution of reflections of crystalline columnar superstructures (Figure 8b).[55] The scattering intensities on the equatorial plane of the pattern are related to the formation of the columnar stacks that are aligned along the fiber direction. Reflections in the wide-angle scattering range located on the meridional and off-meridional are attributed to the intracolumnar packing of the molecules. Thereby, the molecules are titled with respect to the columnar axis what is characteristic for the crystalline phase of such systems. From the position of the off-meridional reflections, a π-stacking distance of 0.37 nm is determined. The pattern of **S*OBT1** also indicates the formation of columns, but interestingly, the π-stacking reflections appear on the equatorial plane instead of the meridional one (Figure 8a). This change is attributed to a switch of the macroscopic alignment of the columnar superstructures in the sample. The location of the π-stacking peak indicates a perpendicular orientation of the **S*OBT1** stacks to the fiber axis. In these structures, the **S*OBT1** molecules are also tilted with a π-stacking of 0.35 nm, which is slightly smaller than that determined for **S*OBT2** due to less sterically demanding side chains. Compounds **S*TBT1** and **S*TBT2** also revealed a perpendicular orientation of the columns with respect to the alignment direction of the fiber. Compared with **S*OBT1** and **S*OBT2**, **S*TBT1** and **S*TBT2** are not tilted within the stacks revealing a π-stacking of 0.36 nm.

A reversed orientation of columnar structures of star- or disc-shaped molecules in mechanically oriented fiber samples was so far triggered either by additional non-covalent forces, such as dipole–dipole interactions, or by an increased molecular aspect ratio.[56,57] Comparing **S*OBT1** and **S*OBT2**, the outer side chains play a major role for the alignment. The additional hexyl side chains change the molecular character of **S*OBT2** into a more disc-like shape that typically orient in their columnar structures along the fiber direction. This behavior is in agreement with the control of the molecular shape and the self-assembly of phenylene-thienylene-based oligomers by the density of the alkyl substituents.[59] The shape of the oligomer was modified from rod- to disc-like by the number of attached substituents. Since the molecular conformation of **S*OBT1** is less rigid and more flexible, the molecules might adapt a more rod-like shape under the mechanical shearing during fiber extrusion and thus orient with the aromatic plane along the alignment direction thereby switching the columnar orientation. Surprisingly, **S*TBT1** and **S*TBT2** do not exhibit such difference in orientation probably due to a high flexibility of the molecular structure of both systems.

### Polymer networks through electrochemical polymerization of S*OBT1 and S*TBT1

As already stated, **S*OBT1** and **S*TBT1** can electropolymerize through oxidative coupling of $C_\alpha$–$C_\alpha$ carbons in terminal thienyl rings to yield a polymeric network. Polymerization of **S*OBT1** through cyclic voltammetry is presented in Figure 9

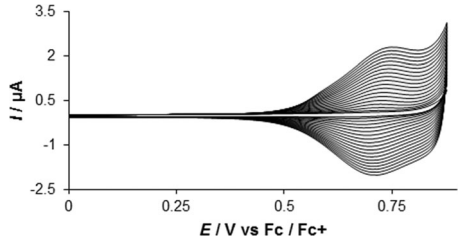


**Figure 9.** Electrochemical polymerization of **S*OBT1** in the cyclic voltammetry mode. Concentration of the monomer: $5\times10^{-4}$ M in 0.1 M $Bu_4NPF_6$/$CH_2Cl_2$; scan rate: 50 mV $s^{-1}$.

whereas analogues scans registered for **S*TBT1** can be found in Figure S4 in the Supporting Information. Uniform, good quality films can be grown either on platinum or ITO electrodes, in the latter case suitable for UV/Vis-NIR spectroelectrochemical investigations.

In the oxidation mode both **poly(S*OBT1)** and **poly(S*TBT1)** yield voltammograms, which are characteristic of p-type doping of conjugated polymers, that is, their oxidation to the polycationic state (see Figure 10). In both cases the appearing redox peaks are superimposed on a capacitive current associated with the formation of a double layer, inherent of the p-doping process.[59,60] Clear anodic peaks with maxima at $E=$ 0.805 V and $E=0.863$ V versus $Fc/Fc^+$ for **poly(S*TBT1)** and **poly(S*OBT1)**, respectively, can be attributed to the transformation of neutral macromolecules into polycations. Upon reverse scan the corresponding cathodic peaks appear at $E=$ 0.740 V and $E=0.803$ V. Easier oxidation of **poly(S*TBT1)**, as compared to **poly(S*OBT1)**, indicates lower IP of the former. The same trend is observed in linear alternating copolymers consisting of oxa- or thiadiazole and oligothiophene.[40] Electrochemical data of **poly(S*TBT1)** and **poly(S*OBT1)** are collected in Table 5.

The polymerization process strongly influences the IP values of the resulting products, which are lower by about 250 meV for **poly(S*OBT1)** and **poly(S*TBT1)** with respect to the corre-

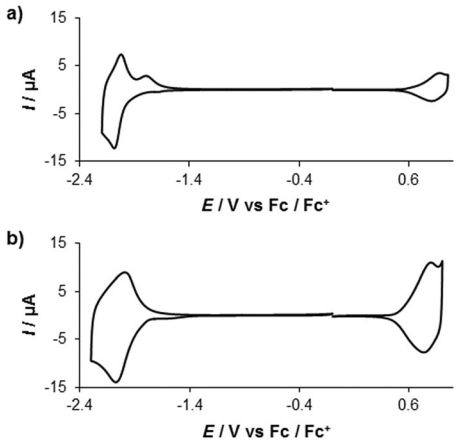


**Figure 10.** Cyclic voltammograms of electrochemical polymerization products registered in monomer-free 0.1 M $Bu_4NPF_6/CH_3CN$; scan rate: 50 mV $s^{-1}$: a) **poly(S*OBT1)**; b) **poly(S*TBT1)**.

**Table 5.** Electrochemical parameters of **poly(S*OBT1)** and **poly(S*TBT1)** derived from cyclic voltammograms. Optical gap is given for comparison.

| Compound | $E_{ox,onset}$ [V] | $E_{red,onset}$ [V] | IP[a] [eV] | EA[b] [eV] | $E_g$(electro) [eV] | $E_g$(opt) [eV] |
|---|---|---|---|---|---|---|
| **poly(S*OBT1)** | 0.65 | −1.93 | 5.45 | −2.87 | 2.58 | 2.28 |
| **poly(S*TBT1)** | 0.51 | −1.84 | 5.31 | −2.96 | 2.35 | 2.13 |

[a] Calculated according to equation IP (eV) $= |e|(E_{ox,onset} + 4.8)$. [b] Calculated according to equation EA (eV) $= -|e|(E_{red,onset} + 4.8)$.

sponding monomers. The reduction process is also affected by the electrochemical polymerization, however, to a lesser extent, lowering the EA values of **poly(S*OBT1)** and **poly(S*TBT1)** by 80 and 35 meV, respectively, as compared to the corresponding monomers (compare Tables 2 and 5). Reduction to a radical anion, which is totally irreversible in the monomers (**S*OBT1** and **S*TBT1**), becomes quasi-reversible in the polymerization product (compare Figures 2 and 10). For **poly(S*TBT1)** one reduction peak with a clear maximum at −2.048 V versus $Fc/Fc^+$ is registered with the corresponding oxidation peak at −1.980 V. Similarly, in the cyclic voltammogram of **poly(S*OBT1)** one reduction peak is present at $E =$ −2.094 V, which, however has two anodic counterparts at −2.023 V and −1.786 V upon reverse oxidation. The double-step oxidation of the nascent radical anions, especially in view of large separation of both cathodic peaks, may indicate a complexity of this process involving electrochemical–chemical acts. Finally, it should be stated that electrochemical band gaps of **poly(S*OBT1)** and **poly(S*TBT1)** are significantly larger than the band gaps of linear alternating copolymers consisting of oxa- or thiadiazole and oligothiophenes.[40,61] This may indicate that the effect of the band gap increase has its origin in the complex topology of the formed polymeric network, which reduces the planarity and by consequence makes the conjugation more difficult to achieve.

Before discussing specific cases of **poly(S*OBT1)** and **poly(S*TBT1)**, it is instructive to describe general features of the spectral changes induced by electrochemical reduction or oxidation of conjugated polymers. Typically, these processes involve bleaching of the π–π* band, characteristic of the neutral state, with concomitant growth of new bands ascribed to polyanionic or polycationic states, which appear at higher wavelength. At the potential of the end of the reduction (or oxidation) peak in the cyclic voltammogram, the π–π* band is usually completely bleached. This is the case of linear, alternating copolymers of oxa- or thiadiazole and oligothiophenes.[40,61]

**Poly(S*OBT1)** and **poly(S*TBT1)** behave, however, differently. In the case of **poly(S*OBT1)** the first spectral changes, induced by its oxidation to a polycationic state, appear at $E =$ 0.65 V, in good agreement in the onset of the anodic peak in the cyclic voltammogram of this polymer. With increasing working electrode potential two bands, ascribed to the polycationic state appear at 1223 nm and 733 nm. Note that the π–π* band shows high intensity even at potentials where its bleaching should be complete, for example, at $E = 0.90$ V.

Upon reduction of **poly(S*OBT1)** two bands attributable to the polyanion state appear at 1290 nm and 762 nm; the bleaching of the π–π* band is also incomplete, similarly as in the case of the oxidation process. Clear isosbestic points observed in Figure 11 a and b unequivocally show that the electrochemical oxidation or reduction of **poly(S*OBT1)** result in mutual interconversion of the neutral and polyionic states. Spectroelectrochemical behavior of **poly(S*TBT1)** is qualitatively the same (see Figure 11 c, d). These rather unusual spectral responses of **poly(S*OBT1)** and **poly(S*TBT1)** to the working electrode potential change indicate that at a certain concentration of charge (positive or negative) imposed on the polymer network, its further electrochemical oxidation (or reduction) is impeded. Moreover, this imposed charge renders unoxidized segments of the network less planar as manifested by the hypsochromic shift of the non-bleached π–π* band. Evidently, complete oxidation (reduction) of a conjugated polymer star-shaped network is more difficult than a linear polymer chain.

## Conclusion

We have elaborated a convenient and efficient method of the preparation of star-shaped donor–acceptor molecules consisting of a benzene central unit and three symmetrically-attached arms of thia- or oxadiazole substituted with alkyl- or dialkylbithiophene. All studied molecules show blue photoluminescence in solution; they are also electroluminescent and in the guest–host light-emitting diode configuration, with 1,3-bis(*N*-carbazolyl)benzene as a host, they emit either bluish (oxadiazole derivatives) or green (thiadiazole derivatives) light. Due to their three-fold symmetry, compatible with that of the graphene layer, they readily self-assemble in monolayers deposited on highly oriented pyrolytic graphite, as evidenced by scanning tunneling microscopy (STM). The derivatives are also processable and can be extruded in a form of fibers exhibiting highly ordered supramolecular organization. These derivatives, whose $C_\alpha$ position in the terminal thiophene rings is not blocked by an alkyl substituent, can electrochemically polymerize to yield a polymer network. The obtained networks are am-

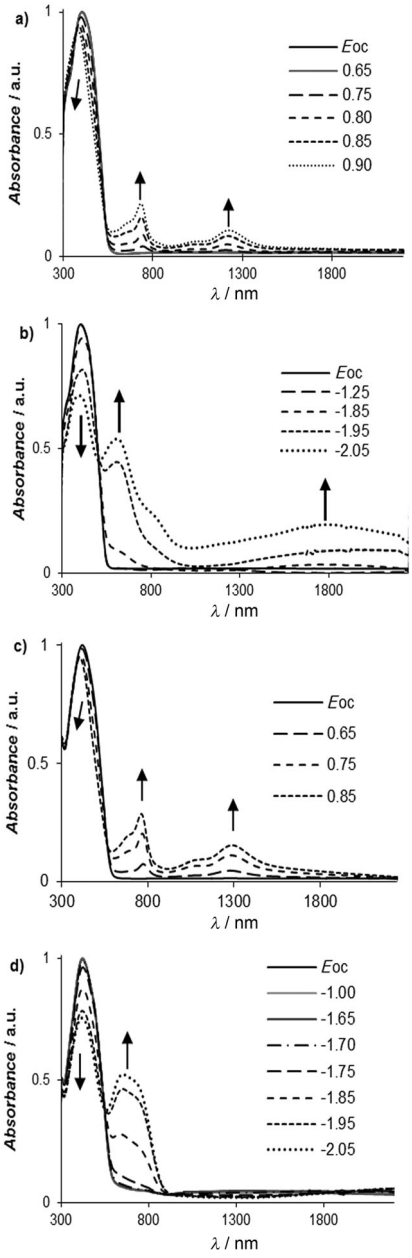


**Figure 11.** UV/Vis-NIR spectra of **poly(S*OBT1)** and **poly(S*TBT1)** films deposited on an ITO electrode. a) Spectra of **poly(S*OBT1)** registered at step-wise increasing working electrode potentials (p-doping mode); b) spectra **poly(S*OBT1)** registered at step-wise decreasing working electrode potentials (n-doping mode); c) spectra of **poly(S*TBT1**) registered at step-wise increasing working electrode potentials (p-doping mode); d) Spectra **poly(S*TBT1)** registered at step-wise decreasing working electrode potentials (n-doping mode), where $E_{OC}$ = open circuit potential. Electrolyte: 0.1 M $Bu_4NPF_6/CH_3CN$; *E* versus $Fc/Fc^+$.

bipolar in character and can be oxidatively (p-type) and reductively (n-type) doped, as evidenced by their cyclic voltammograms. UV/Vis-NIR spectroelectrochemical investigations indicate that the network topology of the resulting macromolecular compounds strongly impedes their p- and n-type doping and their large segments remain undoped at potentials corresponding to the end of the doping process.

## Experimental Section

### Instrumentation and materials

The IR spectra were recorded on an Infralum FT-801 spectrometer in KBr pellets for solid or in thin films for liquid compounds. The $^1H$ and $^{13}C$ NMR spectra were obtained in $CDCl_3$ or $[D_6]$DMSO with TMS as an internal standard, using a Bruker DRX 400 spectrometer (400 and 100 MHz, respectively). The elemental analyses were carried out on a Carlo Erba 1106 CHN analyzer. The melting points were determined on a Kofler bench. The reaction course and purity of the products were checked by thin-layer chromatography on Sorbfil UV-254 plates. The plates were visualized with UV light. All chemicals were of analytical grade and purchased from Sigma–Aldrich UV/Vis-NIR.

Solution and thin films UV/Vis-NIR spectra were recorded in chloroform on a Cary 5000 (Varian) spectrometer whereas the emission spectra were measured using an Edinburgh FS 900 CDT fluorometer (Edinburgh Analytical Instruments). Photoluminescence quantum yields were determined using quinine sulfate in 0.05 mol $dm^{-3}$ $H_2SO_4$ ($\varphi_{fl} = 0.51$) as a standard.[62]

### Electrochemical studies and electropolymerization

Electrochemical properties of all four molecules were investigated using cyclic voltammetry (CV). All cyclic voltammograms were recorded in a dry argon atmosphere on an Autolab potentiostat (Eco Chimie) using a platinum working electrode of the surface area of 3 $mm^2$, a platinum wire counter electrode and an Ag/0.1 M $AgNO_3$/$CH_3CN$ reference electrode. The electrolytic medium consisted of the compound studied ($c = 5 \cdot 10^{-4}$ M) dissolved in a 0.1 M $Bu_4NPF_6$/dichloromethane electrolyte. The potential of the reference electrode with respect to the ferrocene redox couple was always measured after each experiment.

The electropolymerization was performed in the same electrolytic medium using either platinum disk or ITO glass as working electrodes. The best quality polymer films were obtained in the cyclic voltammetry-type process. The potential was cycled (scan rate = 50 mV $s^{-1}$) between the neutral state of the growing polymer (lower vertex potential equal to 0 V vs. $Fe/Fe^+$) and the higher vertex potential corresponding to the onset of the monomer irreversible oxidation peak (as shown in Figure 9). In addition, the best uniformity of the layers deposited on the ITO plate was achieved, when the working and counter electrode were placed in the "face to face" geometry.

### STM experiments

Monomolecular layers were prepared by drop-casting from a solution of the investigated compound in hexane ($\approx 2$ mg $L^{-1}$) on a freshly cleaved surface of highly oriented pyrolytic graphite (HOPG, SPI Supplies, USA). The layers dried under ambient conditions were then imaged in air at room temperature by means of an STM system (University of Bonn, Germany).[63] All images were recorded in a constant current mode using mechanically cut Pt/Ir (80:20%) tips. The proposed real-space models of the monomolecular layers were obtained by the correlation of the layer structure deduced from the STM images and the molecular model of the investigated adsorbate determined using the HyperChem software package.

### Diodes fabrication and characterization

Guest/host-type electroluminescent diodes were fabricated by molecular dispersion of either **S*OBT1 or S*TBT1** (1 to 15 wt%) in an one-component matrix consisting of 1,3-bis(N-carbazolyl)benzene (mCP). Poly(9-vinylcarbazole) (PVK) and 2,2′,2″-(1,3,5-benzinetriyl)-tris(1-phenyl-1-H-benzimidazole) (TPBi) were used as hole-transporting layer and hole-blocking layers, respectively. The active layer of ca. 50 nm was deposited on top of an ITO electrode precoated with a PEDOT:PSS layer of about 50 nm thickness and with a PVK layer of about 10 nm thickness. In the subsequent step a TPBi (50 nm) layer and an ultrathin (1 nm) LiF layer were evaporated followed by deposition of an Al layer. The fabricated devices were tested under ambient conditions. Characteristic of OLED devices were conducted in a 10 inch integrating sphere (Labsphere) connected to a Source Meter Unit (and calibrated with NIST calibration lamp).

## *Acknowledgements*

K.K., L.S., S.K., M.Z., and A.P. wish to acknowledge financial support from National Centre of Science in Poland (NCN, Grant No. 2015/17/B/ST5/00179). A.S.F. and A.S.K. acknowledge partial financial support from the Russian Foundation for Basic Research (15-43-04313-Sibiria-a) and (16-33-00340 mol_a). This work has been also supported by the European Union in the framework of European Social Fund through the Warsaw University of Technology Development Programme, realized by Center for Advanced Studies, granted for K.K. The Gaussian 09 calculations were carried out at the Wroclaw Centre for Networking and Supercomputing (WCSS) Wroclaw, Poland. http://www.wcss.wroc.pl, under computational Grant No. 283.

**Keywords:** electron transport · host–guest systems · self-assembly · semiconductors · supramolecular chemistry

[1] F. Cherioux, L. Guyard, P. Audebert, *Chem. Commun.* **1998**, 2225 – 2226.
[2] A. Pron, P. Gawrys, M. Zagorska, D. Djurado, R. Demadrillea, *Chem. Soc. Rev.* **2010**, *39*, 2577 – 2632.
[3] S. A. Ponomarenko, S. Kirchmeyer, A. Elschner, B. H. Huisman, A. Karbach, D. Drechsler, *Adv. Funct. Mater.* **2003**, *13*, 591 – 596.
[4] K. H. Kim, Z. Chi, M. J. Cho, J. Jin, M. Y. Cho, S. J. Kim, J. Joo, D. H. Choi, *Chem. Mater.* **2007**, *19*, 4925 – 4932.
[5] D. C. Kima, N. S. Kangb, J. W. Yub, M. J. Choa, K. H. Kima, D. H. Choia, *Synth. Met.* **2009**, *159*, 396 – 400.
[6] A. Brzeczek, P. Ledwon, P. Data, P. Zassowski, S. Golba, K. Walczak, M. Lapkowski, *Dyes Pigm.* **2015**, *113*, 640 – 648.
[7] P. Ledwon, R. Turczyn, K. R. Idzik, R. Beckert, J. Frydel, M. Lapkowski, W. Domagala, *Mater. Chem. Phys.* **2014**, *147*, 254 – 260.
[8] Y. M. Sun, K. Xiao, Y. Q. Liu, J. L. Pei, G. Yu, D. B. Zhu, *Adv. Funct. Mater.* **2005**, *15*, 818 – 822.
[9] T. Liu, Ch. Prabhakar, J. Yu, Ch. Chen, H. Huang, J. Yang, *Macromolecules* **2012**, *45*, 4529 – 4539.
[10] J. Luo, B. Zhao, H. S. O. Chana, C. Chi, *J. Mater. Chem.* **2010**, *20*, 1932 – 1941.
[11] P. Leriche, F. Piron, E. Ripaud, P. Frère, M. Allain, J. Roncalia, *Tetrahedron Lett.* **2009**, *50*, 5673 – 5676.
[12] H. Muraoka, M. Mori, S. Ogawa, *Phosphorus, Sulfur, and Silicon and the Related Elements* **2015**, *190*, 1382 – 1391.
[13] R. Sheng, Q. Liu, M. Qiu, C. Gu, Zhou, J. Ren, M. Sun, R. Yang, *Chem. Lett.* **2015**, *44*, 291 – 293.
[14] Y. Nicolas, P. Blanchard, E. Levillain, M. Allain, N. Mercier, J. Roncali, *Org. Lett.* **2004**, *6*, 273 – 276.
[15] T. Taerum, O. Lukoyanova, R. G. Wylie, D. F. Perepichka, *Org. Lett.* **2009**, *11*, 3230 – 3233.
[16] Y. Jiang, D. Yu, L. Lu, C. Zhan, D. Wu, W. You, Z. Xiec, S. Xiao, *J. Mater. Chem. A* **2013**, *1*, 8270 – 8279.
[17] Q. Fan, J. Cui, Y. Liu, W. Su, Y. Wang, H. Tan, D. Yu, H. Gao, X. Deng, W. Zhu, *Synth. Met.* **2015**, *204*, 25 – 31.
[18] A. Cravino, S. Roquet, O. Alévêque, P. Leriche, P. Frère, J. Roncali, *Chem. Mater.* **2006**, *18*, 2584 – 2590.
[19] J. Cremer, C. A. Briehn, *Chem. Mater.* **2007**, *19*, 4155 – 4165.
[20] E. Ripaud, Y. Olivier, P. Leriche, J. Cornil, J. Roncali, *J. Phys. Chem. B* **2011**, *115*, 9379 – 9386.
[21] N. Metri, X. Sallenave, C. Plesse, L. Beouch, P. H. Aubert, F. Goubard, C. Chevrot, G. Sini, *J. Phys. Chem. C* **2012**, *116*, 3765 – 3772.
[22] D. Deng, S. Shen, J. Zhang, C. He, Z. Zhang, Y. Lia, *Org. Electron.* **2012**, *13*, 2546 – 2552.
[23] A. K. Diallo, N. Metri, F. Brunel, X. Sallenave, F. Goubard, O. Margeat, J. Ackermann, C. Videlot-Ackermann, *Synth. Met.* **2013**, *184*, 35 – 40.
[24] W. Li, Q. Li, C. Duan, S. Liu, L. Ying, F. Huang, Y. Cao, *Dyes Pigm.* **2015**, *113*, 1 – 7.
[25] P. Zhou, D. Dang, Q. Wang, X. Duan, M. Xiao, Q. Tao, H. Tan, R. Yang, W. Zhu, *J. Mater. Chem. A* **2015**, *3*, 13568 – 13576.
[26] X. Cheng, J. Zhao, C. Cui, Y. Fu, X. Zhang, *J. Electroanal. Chem.* **2012**, *677 – 680*, 24 – 30.
[27] S. A. Ponomarenko, Y. N. Luponosov, J. Min, A. N. Solodukhin, N. M. Surin, M. A. Shcherbina, S. N. Chvalun, T. Ameri, C. Brabec, *Faraday Discuss.* **2014**, *174*, 313 – 339.
[28] X. He, L. Chen, Y. Zhao, S. C. Ng, X. Wang, X. Sun, X. (Matthew) Hu, *RSC Adv.* **2015**, *5*, 15399 – 15406.
[29] Z. H. Zhao, H. Jin, Y. X. Zhang, Z. Shen, D. C. Zou, X. H. Fan, *Macromolecules* **2011**, *44*, 1405 – 1413.
[30] A. S. Kostyuchenko, A. M. Averkov, A. S. Fisyuk, *Org. Lett.* **2014**, *16*, 1833 – 1835.
[31] H. Tashtoush, R. Subaihi, M. Al-Talib, *Magn. Reson. Chem.* **1997**, *35*, 549 – 552.
[32] U. Mitschke, T. Debaerdemaeker, P. Bäuerle, *Eur. J. Org. Chem.* **2000**, 425 – 437.
[33] C. A. Ramsden, *Tetrahedron* **2010**, *66*, 2695 – 2699.
[34] T. M. Krygowski, H. Szatylowicz, O. A. Stasyuk, J. Dominikowska, M. Palusiak, *Chem. Rev.* **2014**, *114*, 6383 – 6422.
[35] S. S. Erdem, G. A. Ozpınar, M. T. Sacan, *J. Mol. Struct.* **2005**, *726*, 233 – 243.
[36] E. Kurach, D. Djurado, J. Rimarčik, A. Kornet, M. Wlostowski, V. Lukeš, J. Pécaut, M. Zagorska, A. Pron, *Phys. Chem. Chem. Phys.* **2011**, *13*, 2690 – 2700.
[37] E. Kurach, K. Kotwica, J. Zapala, M. Knor, R. Nowakowski, D. Djurado, P. Toman, J. Pfleger, M. Zagorska, A. Pron, *J. Phys. Chem. C* **2013**, *117*, 15316 – 15326.
[38] A. S. Kostyuchenko, V. L. Yurpalov, A. Kurowska, W. Domagala, A. Pron, A. S. Fisyuk, *Beilstein J. Org. Chem.* **2014**, *10*, 1596 – 1602.
[39] A. S. Kostyuchenko, G. Wiosna-Salyga, A. Kurowska, M. Zagorska, B. Luszczynska, R. Grykien, I. Glowacki, A. S. Fisyuk, W. Domagala, A. Pron, *J. Mater. Sci.* **2016**, *51*, 2274 – 2282.
[40] A. Kurowska, A. S. Kostyuchenko, P. Zassowski, L. Skorka, V. L. Yurpalov, A. S. Fisyuk, A. Pron, W. Domagala, *J. Phys. Chem. C* **2014**, *118*, 25176 – 25189.
[41] R. A. J. Janssen, L. Smilowitz, N. S. Sariciftci, D. Moses, *J. Chem. Phys.* **1994**, *101*, 1787 – 1798.
[42] H. G. O. Becker, H. Böttcher, F. Dietz, A. V. Elcov, D. Rehorek, G. Roewer, K. Schiller, O. P. Studzinskij, H.-J. Timpe, *Einführung in die Photochemie*, 2nd ed., Thieme, Stuttgart, New York, **1983**.
[43] A. S. Fisyuk, R. Demadrille, C. Querner, M. Zagorska, J. Bleuse, A. Pron, *New J. Chem.* **2005**, *29*, 707 – 713.
[44] T. Jarosz, P. Data, W. Domagala, W. Kuznik, K. Kotwica, M. Lapkowski, *Electrochim. Acta* **2014**, *122*, 66 – 71.
[45] M. A. Baldo, S. Lamansky, P. E. Burrows, M. E. Thompson, S. R. Forrest, *Appl. Phys. Lett.* **1999**, *75*, 4 – 6.
[46] Q. Peng, N. Gao, W. Li, P. Chen, F. Li, Y. Ma, *Appl. Phys. Lett.* **2013**, *102*, 193304-1 – 193304-4.
[47] J. Zapala, M. Knor, T. Jaroch, A. Maranda-Niedbala, E. Kurach, K. Kotwica, R. Nowakowski, D. Djurado, J. Pecaut, M. Zagorska, A. Pron, *Langmuir* **2013**, *29*, 14503 – 14511.

[48] T. Rieth, T. Marszalek, W. Pisula, H. Detert, *Chem. Eur. J.* **2014**, *20*, 5000 – 5006.
[49] J. Shu, D. Dudenko, M. Esmaeili, J. H. Park, S. R. Puniredd, J. Y. Chang, D. W. Breiby, W. Pisula, M. R. Hansen, *J. Am. Chem. Soc.* **2013**, *135*, 11075 – 11086.
[50] M. Lehmann, P. Maier, *Angew. Chem. Int. Ed.* **2015**, *54*, 9710 – 9714; *Angew. Chem.* **2015**, *127*, 9846 – 9850.
[51] S. K. Pathak, R. K. Gupta, S. Nath, D. S. S. Rao, S. K. Prasad, A. S. Achalkumar, *J. Mater. Chem. C* **2015**, *3*, 2940 – 2952.
[52] S. Park, B.-K. Cho, *Soft Matter* **2015**, *11*, 94 – 101.
[53] B. Feringán, P. Romero, J. L. Serrano, R. Gimenez, T. Sierra, *Chem. Eur. J.* **2015**, *21*, 8859 – 8866.
[54] C. Roche, H.-J. Sun, M. E. Prendergast, P. Leowanawat, B. E. Partridge, P. A. Heiney, F. Araoka, R. Graf, H. W. Spiess, X. Zeng, G. Ungar, V. Percec, *J. Am. Chem. Soc.* **2014**, *136*, 7169 – 7185.
[55] W. Pisula, X. Feng, K. Müllen, *Adv. Mater.* **2010**, *22*, 3634 – 3649.
[56] X. Feng, W. Pisula, L. Zhi, M. Takase, K. Müllen, *Angew. Chem. Int. Ed.* **2008**, *47*, 1703 – 1706; *Angew. Chem.* **2008**, *120*, 1727 – 1730.
[57] L. F. Dössel, V. Kamm, I. A. Howard, F. Laquai, W. Pisula, X. Feng, C. Li, M. Takase, T. Kudernac, S. De Feyter, K. Müllen, *J. Am. Chem. Soc.* **2012**, *134*, 5876 – 5886.
[58] A. Mavrinskiy, C. B. Nielsen, J. R. Reynolds, K. Müllen, W. Pisula, *Chem. Mater.* **2011**, *23*, 1939 – 1945.
[59] A. Pron, *P. Rannou Prog. Polym. Sci.* **2002**, *27*, 135 – 190.
[60] J. Heinze, B. A. Frontana-Uribe, S. Ludwigs, *Chem. Rev.* **2010**, *110*, 4724 – 4771.
[61] K. Kotwica, E. Kurach, G. Louarn, A. S. Kostyuchenko, A. S. Fisyuk, M. Zagorska, A. Pron, *Electrochim. Acta* **2013**, *111*, 491 – 498.
[62] R. A. Velapoldi, *Proceedings of Conference, NBS Gaithesburg, National Bureau of Standards*, Washington, DC **1972**, *378*, 231.
[63] M. Wilms, M. Kruft, G. Bermes, K. Wandelt, *Rev. Sci. Instrum.* **1999**, *70*, 3641.

Received: March 1, 2016
Published online on ■■ ■■, 2016

# FULL PAPER

**Bright stars**: Star-shaped conjugated molecules with oxa- or thiadiazole bithiophene side arms were investigated as promising molecules and building blocks for application in (opto)electronics and electrochromic devices (see figure).

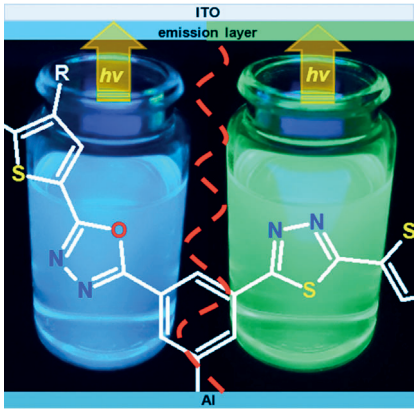


**Host–Guest Systems**

*K. Kotwica, A. S. Kostyuchenko, P. Data, T. Marszalek, L. Skorka, T. Jaroch, S. Kacka, M. Zagorska, R. Nowakowski, A. P. Monkman, A. S. Fisyuk,* W. Pisula,* A. Pron**

■■ – ■■

**Star-Shaped Conjugated Molecules with Oxa- or Thiadiazole Bithiophene Side Arms**